Power Generation via an Autonomous Solar Tower Coupled to a Supercritical CO_2 Brayton Cycle

Abdelkader Beyoud*‡, Najem Hassanain**, Ahmed Bouhaouss*

*Laboratory of Nano Structures, Process Engineering and Environment, Faculty of Sciences, University of Mohammed V, Agdal - Rabat, Morocco

**Materials Physics Laboratory (MPL), Faculty of Sciences, University of Mohammed V, Agdal - Rabat, Morocco

(ay.beyoud@gmail.com, najem.hassanain@gmail.com, Ahmed.bouhaous@gmail.com)

‡ Corresponding Author; Abdelkader Beyoud, Laboratory of Nano Structures, Process Engineering and Environment, Faculty of Sciences, University of Mohammed V, Agdal - Rabat, Morocco, Tel: +212 661 36 55 66,

(ay.beyoud@gmail.com)

Received: 16.03.2019 Accepted:10.05.2019

Abstract- In the context of sustainable development, although concentrated solar energy is an unavoidable alternative for many countries, yet attenuation of solar radiation is a serious obstruction. In addition, the population demands a non-stop energy supply. In this paper, a process is presented. It is made up of a double supercritical CO_2 Brayton cycle coupled to the concentrated solar tower plant, associated with a hydrogen combustion chamber and a solid oxide electrolyzer cell (SOEC) device. In order to continuously produce power supply of 50MW, the exceeding solar energy is managed to produce and accumulate hydrogen alternatively, for a self-consumption at night and/or at the time of insufficiency/absence of solar irradiation. The power production is therefore autonomous around-the-clock in the whole year. In the next phase, a new parameter large solar multiple (L.S.M) is introduced in this paper to size the plant, taking into account five Moroccan regions. Depending on the climate, two rainfall periods are considered; regular and irregular. A one unit of the L.S.M accords 1km^2 of heliostat area in the clear and dry sky conditions. The obtained results demonstrate that for 100% hydrogen self-consumption, the more the atmosphere is clear and dry, the more the production of hydrogen is (5790 tonnes/km^2/a) and the less the surface of heliostat is (1km^2). On the other hand, under the most turbid conditions, the least hydrogen production drops to 2000 tonnes/km^2/a associated with more surface of the heliostat (1.77km^2) as L.S.M value increases twice the unity.

Keywords: Tower power plant, Supercritical carbon dioxide, Hydrogen, Electric production, Atmospheric turbidity, Large Solar Multiple.

1. Introduction

Climate has altered due to anthropogenic activities such as excessive combustion of fossil fuels, industrial processes, deforestation and greenhouse gases released into the atmosphere. The United Nations Conference on Environment and Development, held in Rio de Janeiro in 1992, revolved around the concept of sustainable development, was an international initiative to develop durable strategies for sustainable development as the main global challenge [1]. One of the goals adopted accordingly was to "Guarantee access for all reliable, sustainable and modern energy services at an affordable cost". Deep into this goal is the increase in the share of renewable energies and the provision of sustainable energy services for all particularly in developing countries under the slogan "energy for all".

Solar energy concentration deals with the conversion of solar energy into electricity or heat. Its availability and competitive cost allow widespread accessibility [2]. Currently, thermodynamic solar energy continues to attract growing interest around the world. The installed capacity of the technology has evolved significantly. It has increased tenfold between 2005 and 2017 and it grows at an average of 50% per year during the last five years [3]. Morocco is committed in the United Nations program. It is among the top five countries in the world involved in the development of thermodynamic solar energy conversion [4]. This technology can be very useful especially in remote and arid areas [5]. Indeed, the goals of the 2015 agenda have been confirmed; the summits have advanced towards the sustainability and development as a new agenda 2030 [6]. Hence, any development of energy must verify its integration

into these collective goals of the world. However, like other renewable energies, solar energy provides conditional and variable energy during conversion and immediate operation. One of their major limitations is that they provide discontinuous energies and most of them are unavailable all the time [7, 8]. So the energy storage is an alternative, thanks to its potential role to avoid fluctuations in energy flux from the conversion of renewable energy. In fact, the technologies of molten salt as a mean of storage do not furnish satisfactory solutions. As a matter of fact, the change of their thermo-physical properties allows a limitation of the maximum temperature, in addition to the reduced storage time. Nowadays, hydrogen can be stored for a long time with negligible loss [9, 10]. Moreover, it is the green energy carrier of the future, in case it is produced from a renewable energy source [11]. In fact, hydrogen is the most abundant element of the universe. It is non-toxic, practically clean, and much more efficient than other energy sources [12]. Its combustion allows *149MJ/kg* of the energy amount generated, at 35MPa pressure and at ambient temperature (*298K)* [13]. Thus, it is a useful way to produce electricity having a solar energy source without intermittent behavior [14]. A recent study of the concentration electrolyzer system has demonstrated that solar Fresnel and parabolic technologies can produce respectively 190 and 170tons/km²/day during the highly irradiated month [15]. Excess heat and electricity from concentrated solar technology can be used to produce hydrogen [16-20]. Several studies have looked at various ways to produce hydrogen. Thermochemical cycles have been widely studied since the 1960s, because they have a great theoretical advantage of reducing the temperature level necessary for the dissolution of water while ensuring the release of hydrogen. [21–23].

A design combining a Brayton s-CO_2 recompression cycle with a high temperature integrated steam electrolysis system coupled with an advanced gas cooled reactor was evaluated by Yildiz et al. [24]. They found, for 550 and 700°C, the estimated efficiencies respectively were 50.6% and 52.2%. Hydrogen has a great potential to avoid atmospheric turbidity, and to preserve the environment [25]. Temperature is a stimulant for many chemical reactions. Thermo-chemical production of hydrogen during combustion of a hydrocarbon or pure water requires heat that may give rise to a very high temperature say, 1000°C. In thermodynamic solar energy (heat source), the direct solar irradiation can be concentrated on a solar tower plant to produce very high temperatures, through a supercritical CO_2 Brayton cycle "unlike the other conversion systems as steam Rankine cycles where the maximum temperature can reach 550°C" [26]. In fact, due to the special thermo-physical properties of supercritical carbon dioxide (s-CO_2), it is now used in many scientific and industrial research applications [27, 28]. Angelino initiated the research work on the applications of s-CO_2 in the context of electricity production [29]. Although the efficiency recorded on basic cycles at very low temperatures did not compete with the steam Rankine cycles, it drew more attention to the simplicity and compactness that proved to be advantageous for several applications. In addition, at higher temperatures, the efficiency of the s-CO_2 Brayton cycle improves significantly ahead of steam cycles. Furthermore, Feher suggested an operation above the critical pressure of CO_2, so that the compressor consumes less power, since the fluid is more incompressible at the critical point [30]. Kim et al. analyzed the potential of s-CO_2 cycles using low and high temperature heat sources [31]. Song et al. have proposed a trans-critical CO_2 production cycle powered by solar energy [32]. In comparison point of view, supercritical carbon dioxide Brayton cycle with other power conversion systems, relatively higher efficiency has been confirmed within the mild turbine inlet temperature range (*723-873K*). In literature, comparison of various layouts was made, elucidating the best efficiency for the recompression and regeneration cycles [33–35].

The National Renewable Energy Laboratory (NREL) has recently published a report [36] the U.S. Department of Energy programs of the solar electricity generation technologies of both the solar energy systems (CSP) and solar photovoltaic (PV) systems. It deals with the cost and performance improvement compared to the conventionally generated electricity. When coupled with energy storage systems, photovoltaic and CSP plants can generate electricity on demand. In particular, a photovoltaic device can be coupled with any electricity storage technology, while the CSP is generally associated with thermal energy storage (CSP-TES). Overall, both approaches allow solar power stations to generate electricity after sunset, before sunrise and during turbid atmospheric periods. So, this paper aims at studying the feasibility and possibility of using s-CO_2 as a working fluid of the thermodynamic cycle of a solar tower plant for electricity production in parallel of producing hydrogen. However, high temperatures have two main constraints: the temperature limit of the material, in addition to the radiation heat loss which is proportional to the fourth power of the absolute temperature. In order to ensure the continuity of the energy supply, the lack of solar energy in the production of hydrogen for a potential and efficient energy is taken into account. All sites in morocco had a great potential of direct normal irradiance (DNI), and more suitable for producing hydrogen [37]. In addition the thermodynamic conversion system of solar energy for the electricity production around the clock is an original and creative idea, where the supercritical carbon dioxide Brayton cycle plant is in heart of the process, thanks for its high temperature required for cracking water, besides electricity having an excellent efficiency reaching 52% under the conditions of the simulation.

2. Specific climatic regions of Morocco.

Morocco has a considerable solar potential, with an average global irradiation more than 5,5kWh/m² and sunshine 3300hours/a. The country's strategy is to massively exploit this clean and inexhaustible energy in the future. The stated goal of the Kingdom is to be independent in regard to energy demands. So the methodology in this work concerns the national level according to the particular climate of each region represented by the location indicated in Table1.

It indicates the representative sites of the five climatic regions of Morocco. In addition, the suggested process in this context is aimed at specific conditions in time and space. It refers obviously to a complete, compact system and autonomous, without recourse to other sources of energy, heat or electricity.

Table 1. Moroccan case studies location

Regions	Longitude (° East)	Latitude (° North)	Elevation (m)
Er-Rachidia	-4.43	31.93	1030
S'mara	-11.68	26.74	178
Ouarzazate	-6.94	30.93	1136
Oujda	-1.90	34.68	551
Rabat	-6.85	33.97	78

3. Solar assessment for the case studies location

Optimal sizing and management of energy systems require imperative awareness of the atmospheric health state. The optimization of a solar concentration system plants depends in part on instantaneous values of the regularity rainfall and others meteorological variables; and the part of beam solar attenuated. It seems useful, at first, to study the analytical modeling of the beam solar irradiation, from Ineichen et al. approach, related to the Linke turbidity factor *TL* "a parameter capable of describing the quality of atmosphere". Then to compare it with the satellite-derived databases "CAMS-Rad" covering Morocco.

The instantaneous beam solar irradiation as defined by Ineichen and al. [38] is expressed in equation (1):

$$I_{TL} = \beta . I_0 . \exp(-0.09 . AM . (TL - 1)) \quad (1)$$

Where, the coefficient β is the corrective altitude of the location AM is Air Mass and I_0 is solar beam irradiation at the top of atmosphere. Assessment of beam solar radiation *DNI* is first carried out for a dry and clean atmosphere in analytical approach. Second, the assessment is made in two behaviors of atmosphere, the regular rainfall period, — RRP — the irregular rainfall period — IRP —, as rainfall has an effect on the quality of atmosphere. When the rainfall is regular, the atmosphere is more stable with aerosols, in contrary with the irregular period, where the atmosphere is more disturbed, the sky is not clean, and dust, organic maters and others particles stay longer. The Linke turbidity factor corresponding to each period has already been treated and evaluated in our previous work [39]. Afterwards, in order to validate the approach, the obtained results will be compared and correlated with the measurements of the HelioClim-3 database and discussed.

4. Concept of effective and apparent daytime duration

The specific instantaneous solar direct normal irradiance "hourly" is symbolized by *I**, and day duration from sunrise to sunset in clear and dry sky of atmosphere is the daylight τ_{CDA} and in turbid atmosphere is the daylight τ_{TL}. The daily beam of solar energy undergoes the atmospheric turbidity extinction which is designed by DNI_{TL}. In short, as part of the simple linear model, the seasonal effect on irradiance is omitted. Subsequently, a correlation comparison between DNI_{TL} and DNI_{CDA} on a scatter plot was performed. Then, the estimation of the linear model made it possible to draw the line of regression. The intercept term β_0 is null. So, In order to determine the right amount of heat energy needed during obscure times, the equivalent duration of a turbid day as an effective day is done:

$$\tau_{TL} = \frac{DNI_{TL}}{DNI_{CDA}} \times \tau_{CDA} \quad (2)$$

The irregular rainfall period "IRP", and the regular rainfall period "RRP" are two alternating period in the atmosphere of Morocco; for each of them corresponds a daylight duration $\tau_{(TL,IRP)}$ and $\tau_{(TL,RRP)}$. On the other hand, the effective night-time duration is defined as $\tau_{(night,\ TL)} = 24 - \tau_{TL}$. Thus, the sunshine rate in beam irradiation energy point of view can be defined as (3) as:

$$0 < \chi_{TL} = \frac{DNI_{TL}}{DNI_{CDA}} < 1 \quad (3)$$

The determination of the right and effective daytime is very important for sizing heliostat area of solar tower, and the solar multiple considering only the classical daylight time can perform an under/over sizing of the solar plant. Therefore, a sunshine rate parameter χ_{TL}, can be evaluated for a turbid atmosphere during the regular rainfall period as $\chi_{(TL,RRP)}$, and during the irregular rainfall period as $\chi_{(TL,IRP)}$ against the unity of sunshine rate of the clear and dry atmosphere conditions.

$$\begin{aligned} \tau_{eff} &= \chi_{TL} \times \tau_{CDA} \\ \tau_{(CDA,night)} &= 24 - \chi_{TL} \times \tau_{CDA} \end{aligned} \quad (4)$$

Based on the climate criteria, Moroccan regions are selected across the country as case studies. In the previous work [39], this location has been assessed by the atmospheric Linke turbidity factor responsible to solar attenuation and its dependence on the regularity rainfall. The extraction technique of solar irradiation data from satellite images is commonly used. A validation campaign was conducted by Thomas et al. between HelioClim-3 — HC3D — data compared to high quality measurements of some stations subsequent to the Baseline and the Surface Radiation Network BSRN have demonstrated better and excellent performance [40].

In general, the observation of data shows that HelioClim-3 data are close to *IRP* situation in southern locations and the inverse for the northern. Then the deduction is that the simulation of the location at an irregular rainfall period condition is more adequate in the south of country than the north and vice versa. It appears as an additive factor for the different sites qualifying the turbidity quality of their atmosphere. *TL* is represented during the *RRP* and *IRP* periods in Table 2. Verily, for the highest values of *TL* during periods with irregular precipitation varies between 6.5 and 7 for the sunniest months of the year, such as the months of July and August, which coincides with the longest days of

the year. On average, they exceed 15 hours per day. Yet, the spring equinox is the most significant day for Ouarzazate and S'mara with an *I** recorded respectively of 933Wh/m^2 and 926Wh/m^2 at solar noon; however, the longest days are the solstice summer. On the other hand, the northern regions have a potential during the summer solstice corresponding to the long day of the year. Moreover, Er-Rachidia already has its high *I** in winter solstice. Table 3 shows the statistical analysis results between the Helio-clim3, *I** data assessed in two periods; the regular rainfall period *RRP* and the irregular rainfall period *IRP*. The monthly or the daily bias indicate globally the results are very shorter in the irregular period than the regular, with the highest value is 16.97W/m^2 in Oujda location during the regular rainfall period, and the lowest 4.5 W/m^2 in during the irregular rainfall period.

Table 2. The Linke turbidity factor for the representative Moroccan location in two different times scales the regular Rainfall, and the irregular Rainfall

	Er-Rachidia			S'mara			Ouarzazate			Oujda			Rabat		
Regions	**IRP***	**RRP***	τ*	**IRP***	**RRP***	τ*	**IRP***	**RRP***	τ**	**IRP***	**RRP***	τ**	**IRP***	**RRP***	τ**
Jan.	2,99	3,15	11,00	3,96	3,65	11,71	2,98	3,14	11,00	3,10	3,24	10,81	3,10	3,22	11,00
Feb.	5,53	3,60	11,24	4,22	4,36	12,00	5,54	3,59	11,59	5,51	3,64	11,21	5,44	3,63	11,48
Mar.	4,35	4,41	13,00	5,31	4,67	12,35	4,36	4,40	12,84	4,35	4,42	12,68	4,34	4,38	12,77
Apr.	4,10	4,16	13,53	4,18	4,55	13,50	4,09	4,14	13,17	4,15	4,19	13,83	4,13	4,15	13,30
May.	5,47	4,94	14,00	4,27	4,47	14,00	5,47	4,93	14,74	5,45	4,96	14,13	5,39	4,89	14,87
Jun.	4,38	5,08	14,93	4,09	5,36	14,00	4,34	5,06	15,00	4,45	5,08	15,00	4,40	5,00	15,00
Jul.	6,73	5,31	14,71	5,87	6,18	14,00	6,74	5,31	15,00	6,70	5,37	14,84	6,57	5,27	15,00
Aug.	6,81	5,47	13,74	7,39	5,97	13,81	6,83	5,47	13,52	6,77	5,51	14,00	6,59	5,38	13,81
Sep.	5,45	5,23	12,73	6,86	5,73	13,00	5,44	5,23	12,97	5,43	5,24	12,90	5,33	5,13	13,00
Oct.	4,96	4,06	12,00	4,70	4,38	12,39	4,96	4,04	12,00	4,94	4,08	12,00	4,87	4,02	12,00
Nov.	3,87	3,66	11,53	3,65	4,51	11,00	3,87	3,65	11,23	3,89	3,70	10,57	3,87	3,67	11,00
Dec.	2,97	3,33	11,00	4,02	3,75	11,00	2,99	3,32	11,00	3,03	3,41	10,00	3,04	3,39	11,00

* Linke turbidity factor pour the considered period.
** The *CDA* daytime duration τ.

The NRMSE key indicator indicates the data are low percentage, around 3% monthly and an average of 10% daily, as the turbidity factor used is monthly averaged. The analysis of the monthly uncertainties which involves the *I** data in the *IRP* period is very close to the *HC3D* measurements in 2016.

Turbidity factor, which is the most suitable for the simulation, and estimating the effective day time, is that of this period and can be perfectly suited to sizing the heliostat solar field of the tower plant. The assessment of the hydrogen production capacity was necessary for the production of electricity during the night and the moment of weakening beam irradiation by atmospheric disturbance in Morocco. In particular, if the annual average data are used, then the later will be comparable.

Overall, the effective daylight is the time duration for collecting and exploiting energy, lies between 30% et 34% lost by the atmospheric turbidity, except the obscures times representing the night time duration. In general, only 20% of energetic hours in total during a year must supply the 80% hours remained.

5. High temperature electrolysis

Before to begin the process, in this section, it is important to emphasize that high temperature electrolysis "THE" is a phase occurring in the device composed with several electrolytic cells assembled. — Solid Oxide Electrolysis Cells — "SOEC-THE". This device has the ability to decompose the water molecules at high temperature, thus evidencing a great potential to produce hydrogen in an efficient way at low cost. In fact, the enthalpy required for the decomposition of water is provided by both electricity and heat "less expensive than electricity alone". In accordance with the kinetic approach related to overvoltage phenomena, the ohmic losses decrease when the temperature increases, as long as the cracking of water using the heat energy only requires temperatures exceeding 2500°C. It is feasible only when the free enthalpy is null.

Table 3. Daily statistical analyzed results regular and irregular rainfall periods.

Regions	**MBE [W/m²]**		**RMSE**		**Test Statistical**		**NRMSE [%]**	
	RRP	**IRP**	**RRP**	**IRP**	**RRP**	**IRP**	**RRP**	**IRP**
Er-Rachidia	10,7	5,1	56,0	59,9	9,09	4,0	6,7	6,7
S'mara	10,4	10,1	58,5	59,4	8,43	8,0	9,9	9,7
Ouarzazate	10,2	4,7	62,4	61,8	7,74	3,5	8,7	8,1
Oujda	17,0	11,8	76,5	74,3	10,7	7,6	12,4	11,6
Rabat	13,4	8,3	74,1	70,3	8,62	5,6	13,2	12,3

Table 4. Monthly statistical analyzed results regular and irregular rainfall periods.

Regions	**MBE [W/m²]**		**RMSE**		**Test Statistical**		**NRMSE [%]**	
	RRP	**IRP**	**RRP**	**IRP**	**RRP**	**IRP**	**RRP**	**IRP**
Er-Rachidia	10,6	5,0	30,4	37,6	3,1	1,1	2,2	2,2

S'mara	10,2	10,0	32,9	34,6	2,8	2,5	2,5	2,6
Ouarzazate	10,1	4,5	33,8	33,2	2,6	1,2	2,5	2,0
Oujda	16,9	11,7	45,5	41,6	3,4	2,5	3,8	3,0
Rabat	13,4	8,2	39,7	32,2	3,0	2,2	3,1	2,2

Figure 1 shows that the total amount of enthalpy required for the decomposition of the water molecules in the liquid phase is about 285KJ/mole, which decreases to 243KJ/mole in the vapor phase.

At the optimal operating conditions, through a low-concentrated electrolyte, the best alkaline water electrolysis performance (Cell-efficiency, ≈50%) is attained with the high-voltage and the low currents, for the considered power. The advantage of having low concentration is that it requires low-maintenance on the cell and needs less amount of electrolyte [41].

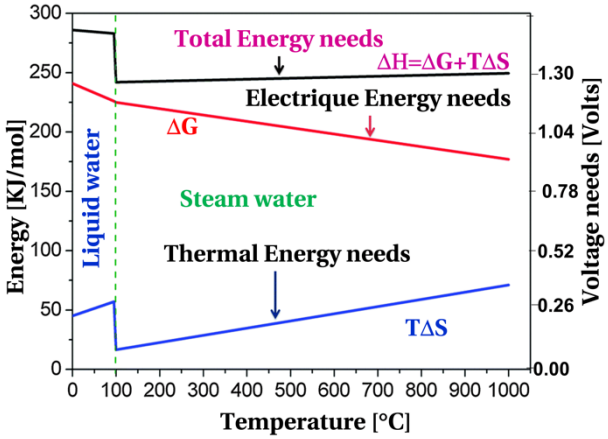

Fig. 1. Complementary of electric energy and thermal energy.

Compared to alkaline electrolysis and membrane electrolysis, high temperature electrolysis shows only progress at all levels, 100% guaranteed efficiency, uses non-noble catalysts, but its durability is short because the operating temperature is high. The increase in efficiency is also particular even during the allo-thermal process where the conditions of operation of voltage and temperature are brought into play, the device of the SOEC operates with a voltage lower than the voltage of the thermo-neutral (1.29V) on the one hand, and on the other hand, in relation to the operating temperature, the total efficiency of the allo-thermal process can reach or more than 50%. This is much better than alkaline water electrolysis.

The temperature plays a balancing role between decreasing the demand for electrical energy and increasing the demand for thermal energy. The free enthalpy ΔG goes from 1.2volts at 100°C to less than 0.9volts at 1000°C, while heat needs goes from 20KJ/mole at 100°C to nearly 74KJ/mole at 1000°C. The interactivity between temperature and electric current in this process would result in each process taking advantage of the other, pulling a high-temperature flow part during the overheating of the design point supercritical carbon dioxide cycle layouts coupled to solar tower plant.

6. Configuration system including s-CO_2 Brayton cycle

Now, the combined cycles with the integration of solar energy for the electricity generation process are the more efficient and are the most effective method from a thermodynamic point of view [42]. A solar tower plant is considered to produce hydrogen through a supercritical carbon dioxide Brayton cycle for two mains motivations. The first one is the pertinent thermal cycle efficiency performed of its recompression layout reach to Carnot efficiency and the second it can provide a very high temperature. This valuable temperature is beneficial for electrolysis HTE operation for producing hydrogen. In Figure 2, the suggested layout has the block 1 which is similar to block 2, and they are two re-compression s-CO_2 Brayton cycles, where in each one, the flow of the fluid has split into two streams before entering the cooling process. One joined to the main compressor via the cooler and the other leaves the exchanger to enter in the secondary compressor.

Indeed, the work of the compressor is thereby reduced and the system loses less heat, which results in the improvement of the thermal efficiency of this cycle. This has also a consequence on the increase of the inlet temperature of the turbine. However, the unstable output power, in that the solar irradiation has a variability according to the atmospheric conditions, the contribution of heat to the s-CO_2 was not constant, which can fall of the threshold fixed for the thermal cycle power. Then this gap can be compensated by the combustion of existing hydrogen in the reserves or in the opposite case, to produce some quantities to accumulate in these reserves of hydrogen in order to obtain a stable power all the year. In addition, the heated process runs in the block0 where the supercritical carbon dioxide fluid is divided into three parts at the arrival. The block, composed by the tower solar receiver and the hydrogen combustion system mounted in series. In order to perform a stable power output, a large part is sent to the main recompression cycle (Block 1). A medium part is sent to the similar secondary cycle (block 2) for producing a small power to feed electrolyzer by means of an AC/DC converter (block 4), that allows the electricity supply to the High Temperature Electrolysis -HTE- block (block 5). The HTE receives the water vapor heated between 700°C and 1000°C fed by a heat exchanger via the last part of the flow (block 3).

So, the design gross power that allows the conversion of immediate electricity were defined at 50MWe, through two of supercritical CO_2 Brayton cycles with recompression, at pressure 20MPa at turbines inlet temperature (TIT) of 1273K. Others parameters are presented in the Table 5.

$$0 \le \sum_{365}\left[1-\frac{Q(net,ctp)}{Q(net,abs)}\right] \le \varepsilon \tag{5}$$

The overall efficiency of cycle is defined as:

$$\eta_{net} = \frac{\sum_{Cycle} W_T - \sum_{Cycle} W_C}{\sum_{Heat} Q_{(net,ctp)}} \tag{6}$$

Where Q(net,abs) is the heat of the absorber tower, throughout clean and dry atmosphere, add to heat fraction provided from hydrogen to fulfil the deficit during the extinction of beam solar radiation, in order to maintain the turbine at the rated capacity. The heat cycle thermal power rate is Q(net,ctp) , must be always constant, ε is the annual self-consumption rate and, W_T is the turbine power output, W_C is the compressors power consumed, taking into account the polytropic efficiencies.

The result in which Matlab was used, Aspen's Hysys V08 software [43] was also employed to verify the simulations. The validation of the model of the cycle has been validated by block "2 and 3" separately, by referring to the approaches described by the model of Moisseytsev and Dostal [44, 45]. The present model gives results that are comparable with the literature, following the set of equations of states implemented for the different applications and software chosen. The works that used the same comparison software as ours [46] shows a compliance rate of +0.01% at the low temperature level and + 6% at the high temperatures, since the data relating to the high temperatures were compared by extrapolation.

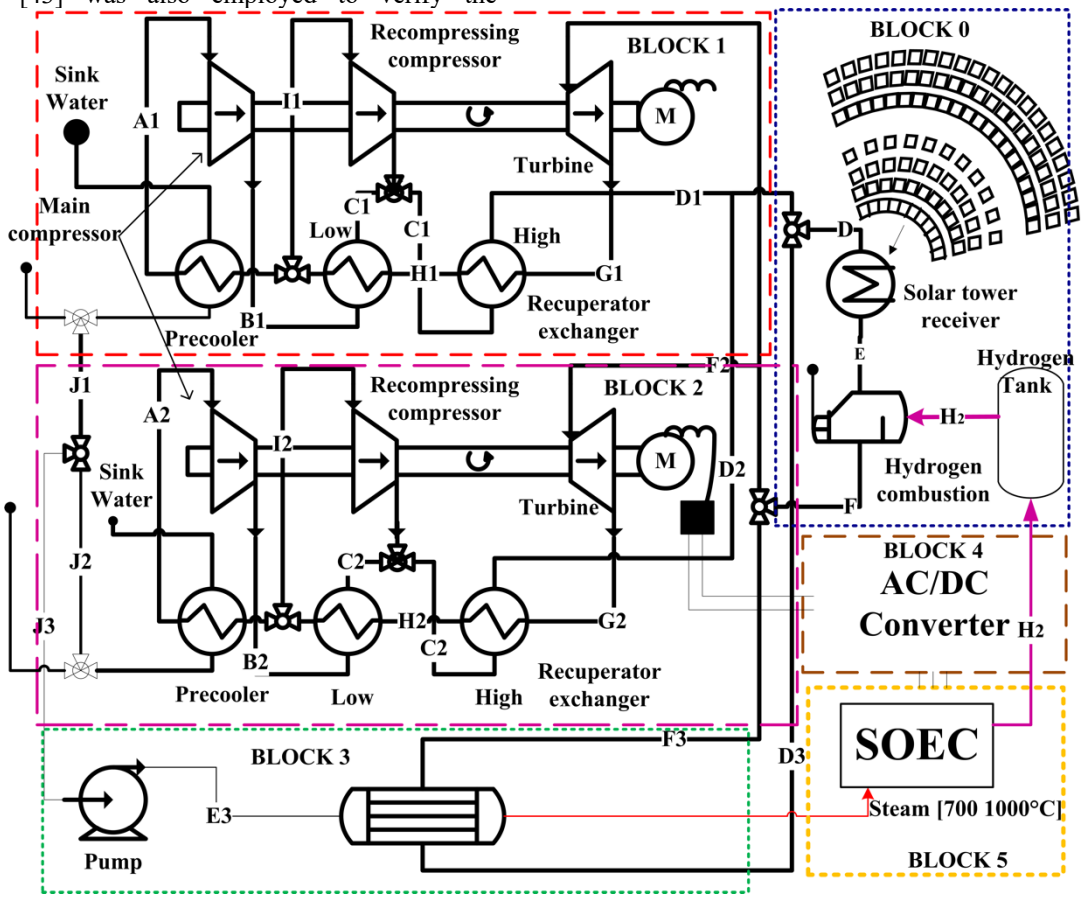

Fig. 2. Recompression Supercritical Carbon Dioxide Brayton, coupled to Solar Tower and the hot water/electric power feeding to thermolysis SOEC.

Figure 3 also shows the increase in thermal efficiency, with the conditions of the minimum pinch temperature in the heat exchanger and the optimum pressure ratio. Also, the turbine inlet temperature range of 550°C to 1000°C including of course the temperature range of electrolysis [700-1000°C] was chosen for the determination of thermal efficiency. In addition, the pressure drop is neglected in all the steps of the process. Indeed, the monotony of the increase in efficiency follows the temperature at the inlet of the turbine reaching the Carnot efficiency. The high temperature was also analyzed.

For a given turbine inlet temperature *TIT*, the thermal efficiency is at an optimum pressure ratio of 2.67 however, the pinch temperature in the heat exchanger was kept as low as possible. Moreover, for a given efficiency of the heat exchanger, in accordance with the minimum possible and acceptable pinch temperature, the high pressure increase in parallel to increase the turbine inlet temperature.

Table 5. Basic parameters considered of design point and operating parameters used for the central tower.

Design point parameters	Value	Unit
Design turbine gross power	50	MWe
Gross to net conversion factor	0,9	
Cycle thermal efficiency	0,51	
Cycle thermal power	98	MWth
Design point DNI	100	W/m2
Absorber thermal power	98	MWth
s-CO2 Hot Temperature	1237	K

s-CO2 Cold Temperature	304,1	K
Heating Pressure	25	MPa
Reheating pressure	13	MPa
Pressure ratio (Optimum)	3,333	Unit

Figure4 shows seven curves, as an example, the considered location is Rabat, and the given date is January the first 2016, because the cycle is a machine independent from location where it is installed. The *I** simulated in red dashed curve is compared to the data of the same day extracted from HelioClim-3D. The green dashed curve is in entire concordance with the data with a correlation factor of $R^2 = 0.9795$. The optical efficiency and of the heliostat field, are computed at an optimal of the reflective area corresponding to 1km^2, design point of $250W/m^2$, solar multiple of S.M=1 and others thermal parameters are indicated in Table 5.

So the thermal $Q(sol,in)=\eta(helio)\bullet A(helio)\bullet I^*$ represented by the black curve, the heat lost from the absorber in receiver placed on the top of the tower is a sum of the radiation heat and convection heat [47, 48]. Purple curve in the bottom and the net heat net conform the absorber thermal power at design point.

Therefore, the *DNI (I*)* data used was simulated by time step. The total incident energy traveled from the mirrors of heliostat field arrives at receiver placed on the top of the tower then the useful energy was absorbed, and the losses by radiation and convection were omitted. For comparison, the *DNI* data are also illustrated and the evolution of the useful energy help distributor splitter to predict the management manner of the excess of heat flow, by means of supercritical CO_2. In reality, when the machine runs from the heat conditions of the design point, no flux flows to the heat exchanger. The distributor splitter extracts part of the flow and send it to this exchanger and consequently to the SOEC.

Figure 5 portrays the simulated heat growing at two *TIT* 700°C and 1000°C, the inner subplot began constantly from the design point heat around 100MW. The same fraction of evolution and one part of the supercritical carbon dioxide is extracted for the benefit of water exchanger, as a fraction of the heat flow. The outer subplot shows the mass flow of water heated in kg/s at two temperatures.

The low *TIT* allows a lot of energy for heating the same amount of water is taken to heat the water in a heat exchanger at 1000 °C.

The cycle has two turbines, one to operate the electric generator of *50MWe* with an efficiency of 90%, a second turbine to move the small electric generator until to *1MWe* to supply the electrolysis via a converter device *AC/DC*.

In the light of the simulated curves, in the case where the energy of the solar field collected by the absorber of the tower exceeds the heat required by the thermal cycle power, then the surplus of 25, 50, 75 and 100MW will be raised through the automatic valve, and transferred to the system exchanger and electrolyzer with the rates respectively of 20, 28, 45, and 50%. Then the amount of water heated to 1000°C is respectively 10, 13, 23, and 25Kg/s and thereafter in a complete reaction, the hydrogen production is respectively 8, 10.4, 18.4 and 20 tonnes/hour. In short, for a very sunniest day, with an average surplus of 100MW for an average day of 10 hours (surplus time), 200 tonnes/km²/ day is produced.

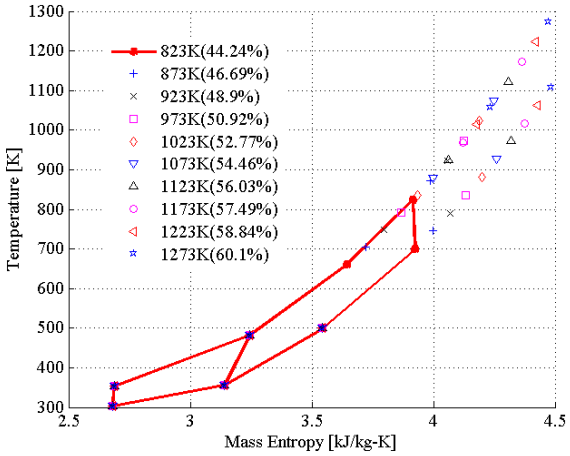

Fig. 3. The temperature – entropy diagram comparison of recompression s-CO_2 Brayton cycle and efficiency *TIT* range [550-1000°C]. The full line in red corresponds to the literatures results.

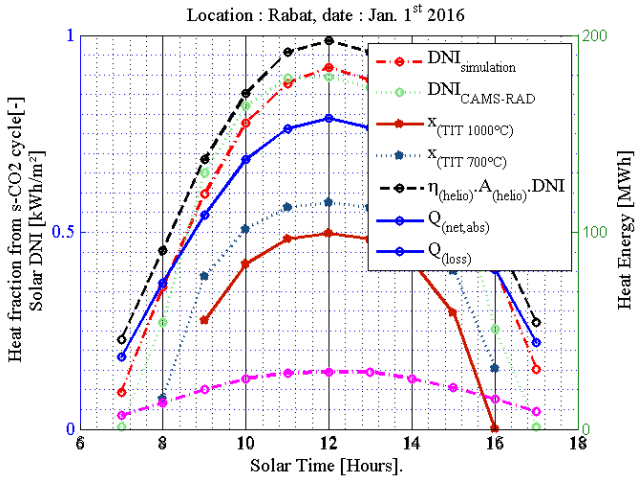

Fig. 4. The split flow ratio, of s-CO_2 for heating water at temperatures 700 °C and 1000 °C are illustrated in the middle, detailed in the next section.

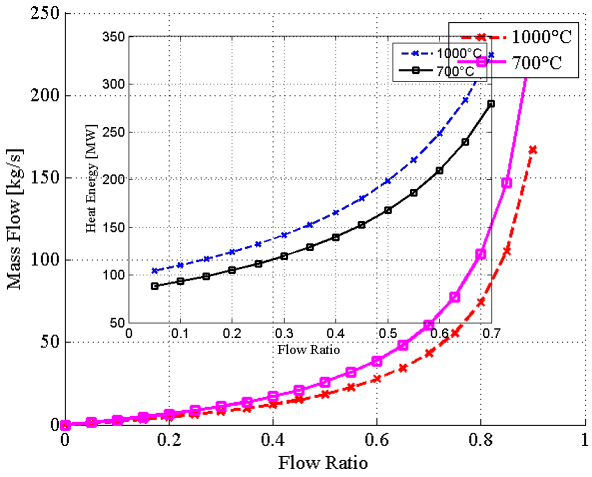

Fig. 5. Water mass flow conforming the growing of solar heat managed by the splitter of s-CO_2 flow ratio.

7. Large Solar multiple (L.S.M)

A large solar multiple is simply the habitual S.M extended to include solar heat equivalent for night. Regardless of the cost of installation and exploitation, when the solar potential is high, the control system cannot handle an overproduction of thermal energy through an oversized reflective surface, exceeding the needs of the cycle thermal power block. A proposed solar tower plant with a nominal power of 50MWe focuses on the size and the design. So, the process initiated by optimization of heliostat solar field, the reflective area for a system at a given location.

In the present approach, optimization of the solar field must satisfy some necessary conditions: the more significant effective day time during which the solar field produces more heat to power, the power supply to its nominal capacity, taking into account, of course, the equivalent night time duration and the minimization of installation, maintenance and operating costs during its lifetime. In addition to the efficiency of production from heat to hydrogen and the efficiency of conversion from hydrogen to heat for nocturne power needs.

The large solar multiple L.S.M is a key able to verify this hypothesis, in the context of hydrogen production for the nocturnal need. For computing the optimal large solar multiple, the process was simulated by Matlab. In order to compute the large solar multiple needed for immediate electricity production, and/or producing hydrogen, the optimization of the solar field geometry, number of heliostat, and the reflective surface of the solar tower, is done by the simulator of SAM [49].

The solar multiple L.S.M = 1 is conformed to 1km^2 of reflective surface. It is the solar multiple without taking into account storage, compensation of atmospheric attenuation and nocturnal power need. 24 hours is considered.

The solar multiple formulated by the Equation (7) relating to the nocturnal needs in energy in addition to the deficits due to the solar attenuation of the day.

$$L.S.M = \left[2 - \eta_C\left(H_2\right).\eta_P\left(H_2\right)\right] \times S.M_{daytime} \quad (7)$$

$$S.M_{daytime} = \frac{Q_{(net,abs)}}{Q_{(net,ctp)}} \quad (8)$$

$$S.M_{(T_L,daylight)} = \alpha_{(T_L\ daylight)} \times S.M_{daytime} \quad (9)$$

The efficiencies of production and conversion from hydrogen to energy and vice versa are defined respectively by $\eta_{p(H_2)}$ and $\eta_{c(H_2)}$. Thus, equation (7) is a monotonic function of an annual sunshine rate. As a result, in the large solar multiple, the high value the L.S.M is obtained when the atmosphere location is more turbid $\chi_{TL} << 1$.

$$\alpha_{(T_L,daylight)} = \frac{\sum_{i=1}^{N} \chi_{(T_L,i)}.\tau_i}{M} \quad (10)$$

With, N and M are respectively the number of days and hours depend on leap or ordinary year.

Figures 6, 7, 8, 9 and 10 portray the monthly details of self-consumption evolution of hydrogen. The consumption of hydrogen to compensate the deficit of solar radiation begins the day after the cessation of production and lasts one semester. So for normal conditions simulated under *RRP* and *IRP*, the production of hydrogen to fill stocks is usually from spring equinox to summer solstice. The call for reserves are suspended during the turbid months, namely the month of February, with the exception of S'mara whose calls reserves in August and September, known by months of sandstorm.

In the case of CDA conditions, hydrogen production in all selected sites lasts six months, from April to September, and consumption during the rest of the year, with a variation of hydrogen consumption is from 180 tonnes / month to 220 tonnes/month from the south locations to the north ones. In the same way, the angle of declination that forms the vector (centre of the earth - sun) and the equatorial plane of the earth thus defining the maximum of production/ consumption is respectively the summer solstice and the winter solstice and vanishes during the equinox. Straightforwardly, what is produced and stored the day is consumed at night.

In the second case RRP, the period is known as regular rainfall, the process of self-consumption of hydrogen continues at the same pace as the case of CDA with a difference during the summer season when the premature consumption of the stock starts in full summer, before the equinox in the autumn. For all regions are one month behind starting consumption except in the region of S'mara, because the rising of the dust starts in the south and progressively goes up towards the north, particularly the sub-Saharan Sahel belt (our previous work [50]). The enhancement compared to the CDA is due to the L.S. multiplicative parameter which has been sized on the most favourable month, and optimized to cover the hydrogen storage required for a whole year.

In the third case IRP, the period known for irregular precipitation, the aerosols dust and organic matter are too

much present in the atmosphere, the production of hydrogen is ensured only by four months on the spring season and the first month of the summer. The optimization of the L.S.M tends from a unit value towards the double. IRP produce more hydrogen during the higher potential months and consume more of them during the low potential months.

The production is more important for the *IRP* whose maximum fluctuates between 500 tonnes/a, and 600 tonnes/a, for all the regions. This is due to the sizing of the solar field; the large solar multiple is to increase by almost 65% compared to the *CDA*.

The use of the situation of the *CDA*, the central will undersize compared to a real situation. Also, the *H3CD* data validate the numerical approach used in this work, so as to know the characters of the rainfall of each site apart.

All the results concerning the production of hydrogen on a solar heliostat unit km^2 compared to the large solar multiple, with a self-consumption are demonstrated in Fig11.

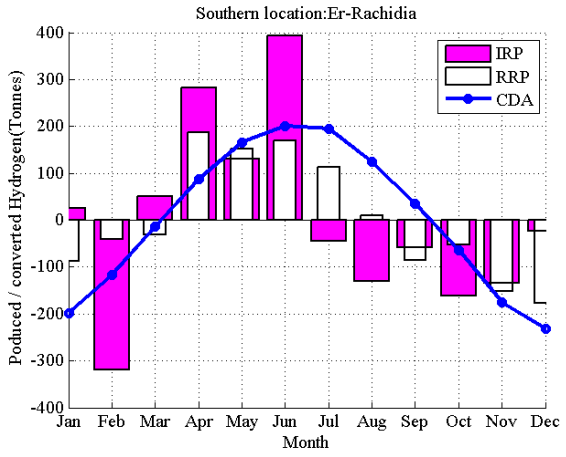

Fig. 6. The self-consumption of amount of hydrogen at Er-Rachidia in different climate conditions.

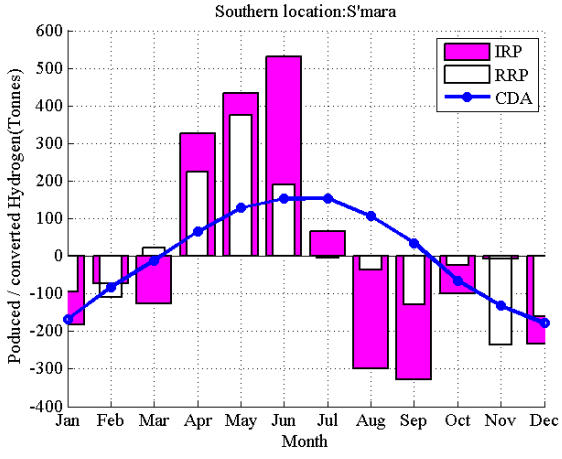

Fig. 7. The self-consumption of amount of hydrogen at S'mara in different climate conditions

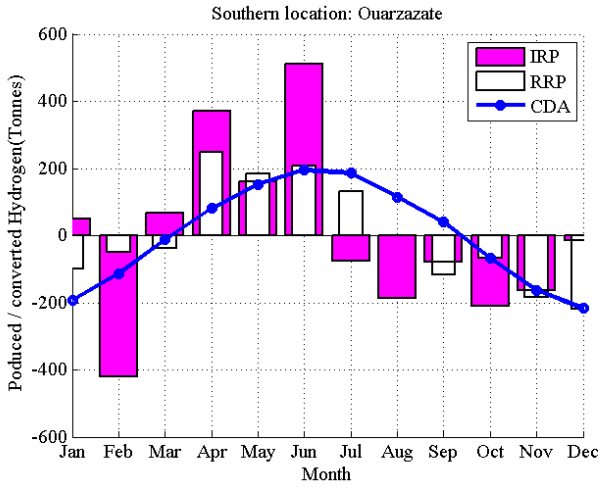

Fig. 8. The self-consumption of amount of hydrogen at Ouarzazate in different climate conditions

So, the L.S.M tends towards unity for all regions under a clear and dry sky of atmosphere, with the production of hydrogen to keep the 50MWe power generation capacities stable all year round. Production starts from the spring equinox and ends on the equinox day of autumn with around 5500 tonnes annually.

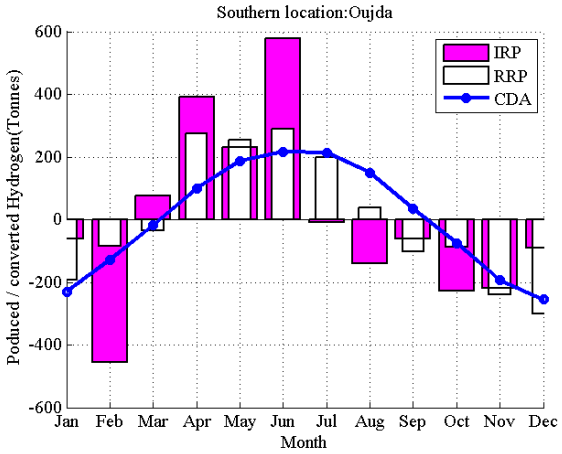

Fig. 9. The self-consumption of amount of hydrogen at Oujda in different climate conditions.

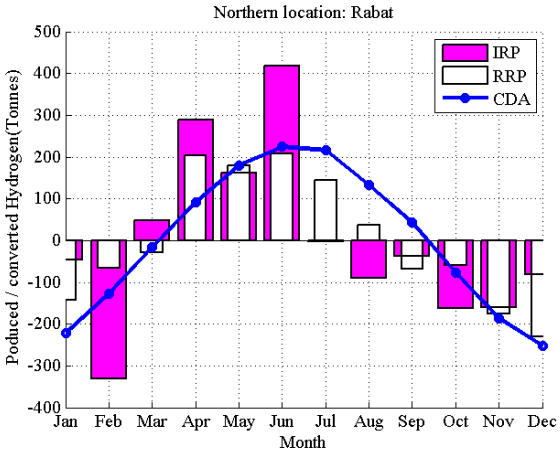

Fig. 10. The self-consumption of amount of hydrogen in Rabat under different climate conditions.

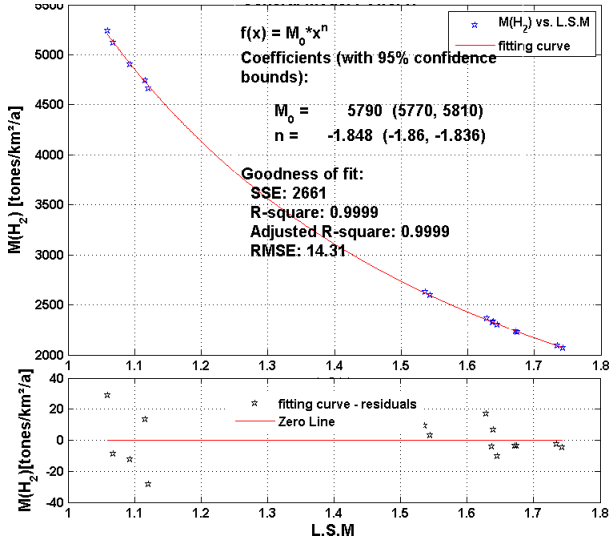

Fig. 11. Correlation of hydrogen production amount and Large Solar Multiple.

Figure 11 shows comparison of hydrogen production amount averaged on 1km^2 and Large solar multiple on the top of the figure with least squares approximation approach, (in the bottom representation of residuals against a zero line). With an R-square value of *0.99* the points *(L.S.M, M(H₂))* are not aligned, but close to some form of hyperbola or rather to a form of power function given as:

$$M(H_2) = M_0.(L.S.M)^n \quad (11)$$

Where, $n = -1.484$ and $M_0 = 5790$ tonnes/km^2/a, is the value of the amount of hydrogen must be produced at the least value of *L.S.M = 1*, and *2069* tonnes/km²/a the maximum of *L.S.M =2*. Thus, this amount obtained with the hyperbola regression above, which is the correlation of amount of hydrogen produced against the values of *L.S.M*.

The amount of hydrogen modeled is plotted against the values calculated for the periods of regular rainfall and irregular periods, for the different climatic regions of Morocco. It can be noticed that the agreement is very good from the unity of *L.S.M* up to *1.75*

Bearing in mind that to ensure the continuity of service of supply of electric energy with a self-consumption rate of almost *100%*. Concerning the *CDA* situation, production of hydrogen is more over than the *IRP* period. In *IRP* where the surface is too large, there are some months with production peaks, other with consumption peaks spaced several months apart. Therefore, the expression 9 can be used to estimate the amount of hydrogen production in accordance with *L.S.M* for a generation, a stable power of *50MWe* around a clock. The calculation of *L.S.M* depends on Linke factor turbidity which can deduce the effective daytime duration, the efficiency of hydrogen production, and the efficiency of hydrogen conversion.

8. Conclusion

In this article, an ingenious process has been introduced. The solar Tower plant can generate electricity on demand, by self-consumption of hydrogen without resorting to thermal energy storage. It is feasible to make an autonomous and independent solar power plant with a capacity of 50 MWe, having continuous production, around the clock.

Its receiver is associated with a double supercritical CO_2 Brayton cycle, the principal one, based on sun power, while the secondary on the surplus of solar energy above the design point, in order to provide an electric current and heat necessary for producing hydrogen.

Thus, an analysis of the attenuation of the beam normal irradiation covering the country was initiated. In addition, two periods of regular and irregular rainfall are considered. They alternate randomly on the Moroccan atmosphere; they are due to climate change on a global scale. Therefore, the beam radiation was attenuated, in relationship with the effective daytime. Afterwards, the amount of energy needed for nightly needs and daily deficits due to turbidity is assessed.

The solar multiple is an important parameter for the sizing of the solar heliostats field with storage, while the large solar multiple introduced in this work also extends to the lack or insufficiency of solar radiation. This can vary from single to double; it is a function of three parameters, the two efficiencies of hydrogen production and conversion added to the annual sunshine rate parameter.

The solar Tower plant can generate on demand non-stop power of 50 MWe, in the case of CDA, in the regular manner, between spring and autumn equinox and during the spring and summer seasons, the more of hydrogen is produced, but during the autumn and winter seasons is consumed. In the IRP case, only three month of spring season is used to produce for the rest of the year. The estimate annual amount of hydrogen self-consumed approximately is 5770 tonnes / km², and 2200 tonnes / km², for the two cases, respectively, beside of the L.S.M tends from unity towards double.

In addition, we find a conversion function between the quantities of hydrogen expressed in tonnes/km^2 and the large solar multiple, which is considered for taking into account the atmospheric conditions.

Finally, from the perspective point of view, the study will be pursued by a comparison with batteries and an in-depth study of the SEOC electrolyzer in the context of the supercritical CO_2.

9. List of abbreviations

DNI : Direct Normal Irradiance
CAMS-RAD /HC3D: Copernicus Atmosphere Monitoring Service Radiation / HelioClim database 3
CDA : Clear and Dry Atmosphere
RRP/ IRP: Regular Rainfall Period /Irregular Rainfall Period
BSRN : Baseline Surface Radiation Network
TL : Linke Turbidity factor
NRMSE: Normalized Root Mean Square Error
RMSE : Root Mean Square Error
MBE : Mean Bias Error

s-CO_2 : Supercritical Carbon Dioxide
CSP : Concentrated Solar Power
CSP-TES: CSP associated with thermal energy storage
THE : High Temperature electrolyzer
L.S.M : Large solar multiple
S.M : Solar Multiple
SOEC : Solid Oxide Electrolysis Cells
TIT : Turbine Inlet Temperature
SAM : System Advisor Model
DOE : U.S. Department of Energy

Acknowledgements

The Authors wish to express his gratitude to Professor Muhammad Azeem Arshad Who provided useful feedback which led to a better presentation of the manuscript. The authors are also grateful to IRESEN for their kind support.

References

[1] J. Drexhage, & D. Murphy, 2010. "Sustainable Development: From Brundtland to Rio 2012. Background Paper Prepared for Consideration by the High Level Panel on Global Sustainability at Its First Meeting", 19 September 2010, UN Headquarters, New York.

[2] Kolb, Gregory J., Clifford K. Ho, Thomas R. Mancini, and Jesse A. Gary, 2011. "Power tower technology roadmap and cost reduction plan." SAND2011-2419, Sandia National Laboratories, Albuquerque, NM7, vol.17, pp.1-38.

[3] Ilas, Andrei, Pablo Ralon, Asis Rodriguez, and Michael Taylor., 2018. "Renewable power generation costs in 2017." International Renewable Energy Agency (IRENA): Abu Dhabi, UAE, pp.1-160.

[4] Z. Jokadar and K. Wade, 2015. "Specific Environmental and Social Impact Assessment Client ACWA Power,", vol. 1, pp.1-220.

[5] Y. Elmaanaoui et D. Saifaoui, 2018. Preliminary Assessment of an Organic Rankine Cycle Power Plant Derived by Linear Fresnel Reflector. International Journal of Renewable Energy Research (IJRER), 8(4), pp.2014-2024

[6] K.W. Robert, T.M. Parris, and A.A. Leiserowitz, 2005. What is sustainable development? Goals, indicators, values, and practice. Environment: science and policy for sustainable development, 47(3), pp.8-21.

[7] R.R., Hernandez, M.K. Hoffacker, and C.B., Field, 2014. Land-use efficiency of big solar. Environmental science & technology, 48(2), pp.1315-1323.

[8] M. Shatnawi, N. A. Qaydi, N. Aljaberi and M. Aljaberi, "Hydrogen-Based Energy Storage Systems: A Review," 2018 7th International Conference on Renewable Energy Research and Applications (ICRERA), Paris, 2018, pp. 697-700. doi: 10.1109/ICRERA.2018.8566903,

[9] I. Ray, T. Chakraborty, D. Roy, A. Datta, and B.K. Mandal, 2013. Production, storage and properties of hydrogen as internal combustion engine fuel: a critical review. Natural gas, 240, p.48.

[10] B., Mohamed, B., Ali, B., Ahmed, L. Salah, and D., Rachid, 2016. Study of hydrogen production by solar energy as tool of storing and utilization renewable energy for the desert areas. International Journal of Hydrogen Energy, 41(45), pp.20788-20806.

[11] O. Bilgin, "Evaluation of hydrogen energy production of mining waste waters and pools," 2015 International Conference on Renewable Energy Research and Applications (ICRERA), Palermo, 2015, pp. 557-561. doi: 10.1109/ICRERA.2015.7418475.

[12] S. Kaya, B. Öztürk and H. AykaÇ, "Hydrogen production from renewable source: Biogas," 2013 International Conference on Renewable Energy Research and Applications (ICRERA), Madrid, 2013, pp. 633-637. doi: 10.1109/ICRERA.2013.6749832.

[13] Burhan, M., Oh, S.J., Chua, K.J.E. and Ng, K.C., 2017. Solar to hydrogen: Compact and cost effective CPV field for rooftop operation and hydrogen production. Applied energy, 194, pp.255-266.

[14] M. Ball, and M., Weeda, 2015. The hydrogen economy–vision or reality?. International Journal of Hydrogen Energy, 40(25), pp.7903-7919.

[15] R., Boudries, 2013. Analysis of solar hydrogen production in Algeria: Case of an electrolyzer-concentrating photovoltaic system. International Journal of Hydrogen Energy, 38(26), pp.11507-11518.

[16] T., Muneer, M. Asif, and S., Munawwar, 2005. Sustainable production of solar electricity with particular reference to the Indian economy. Renewable and Sustainable Energy Reviews, 9(5), pp.444-473.

[17] N., Bidin, S.R., Azni, M.A.A., Bakar, A.R., Johari, D.H.F.A., Munap, M.F., Salebi, S.N.A., Razak, N.S. Sahidan, and S.N.A., Sulaiman, 2017. The effect of sunlight in hydrogen production from water electrolysis. International Journal of Hydrogen Energy, 42(1), pp.133-142.

[18] J. Morel, S. Obara, K. Sato, D. Mikawa, H. Watanabe and T. Tanaka, "Contribution of a hydrogen storage-transportation system to the frequency regulation of a microgrid," 2015 International Conference on Renewable Energy Research and Applications (ICRERA), Palermo, 2015, pp. 510-514. doi: 10.1109/ICRERA.2015.7418465.

[19] M., Fereidooni, A., Mostafaeipour, V. Kalantar, and H., Goudarzi, 2018. A comprehensive evaluation of hydrogen production from photovoltaic power station. Renewable and Sustainable Energy Reviews, 82, pp.415-423.

[20] L. Schlapbach, and A., Züttel, 2011. Hydrogen-storage materials for mobile applications. In Materials for sustainable energy: a collection of peer-reviewed research and review articles from nature publishing group, pp. 265-270.

[21] Yilmaz, Fatih, M. Tolga Balta, and Reşat Selbaş, 2016 "RETRACTED: A review of solar based hydrogen production methods."pp; 171-178.

[22] K. Zeng, and D., Zhang, 2010. Recent progress in alkaline water electrolysis for hydrogen production and applications. Progress in Energy and Combustion Science, 36(3), pp.307-326.

[23] R.E., Chao, 1974, "Thermochemical water decomposition processes". Industrial & Engineering Chemistry Product Research and Development, 13(2), pp.94-101.

[24] B. Yildiz, K. J. Hohnholt, and M. S. Kazimi, 2006, "Hydrogen Production Using High-Temperature Steam Electrolysis Supported by Advanced Gas Reactors with Supercritical CO_2 Cycles," Nucl. Technol., vol. 155, no. 1, pp. 1–21.

[25] D.S., Scott, 2004. Back from the Future: To Build Strategies Taking Us to a Hydrogen Age. In The Hydrogen Energy Transition, pp. 21-32. Academic Press.

[26] C.H., Oh, 2006. Development of a Supercritical Carbon Dioxide Brayton Cycle: Improving VHTR Efficiency and Testing Material Compatibility-Final Report (No. INL/EXT-06-01271). Idaho National Laboratory (INL).

[27] K.H. Kang, and S.H., Chang, 2009. Experimental study on the heat transfer characteristics during the pressure transients under supercritical pressures. International Journal of Heat and Mass Transfer, 52(21-22), pp.4946-4955.

[28] G., Angelino, 1968. Carbon dioxide condensation cycles for power production. Journal of Engineering for Power, 90(3), pp.287-295..

[29] Y. Ahn et al., 2015, "Review of supercritical CO_2 power cycle technology and current status of research and development," Nucl. Eng. Technol., vol. 47, no. 6, pp. 647–661.

[30] E. G. Feher, 1968 "The Supercritical Thermodynamic Power Cycle," Energy Convers., vol. 8, no. 2, pp. 85–90.

[31] Y.M., Kim, C.G. Kim, and D., Favrat, 2012. Transcritical or supercritical CO_2 cycles using both low- and high-temperature heat sources. Energy, 43(1), pp.402-415.

[32] Y. Song, J. Wang, Y. Dai, & Zhou, E. 2012. Thermodynamic analysis of a trans-critical CO_2 power cycle driven by solar energy with liquified natural gas as its heat sink. Applied energy, 92, 194-203.

[33] V. Dostal, M.J. Driscoll, P. Hejzlar, and N.E. Todreas, 2002, January. A supercritical CO_2 gas turbine power cycle for next-generation nuclear reactors. In 10th International Conference on Nuclear Engineering (pp. 567-574). American Society of Mechanical Engineers.

[34] M. Kulhánek and V. Dostál, 2011, "Supercritical Carbon Dioxide Cycles Thermodynamic Analysis and Comparison," Proc. SCCO2 Power Cycle Symp., pp. 1–12.

[35] C. K. Ho and B. D. Iverson, 2014 "Review of high-temperature central receiver designs for concentrating solar power," Renew. Sustain. Energy Rev., vol. 29, pp. 835–846.

[36] Murphy, Caitlin, Sun, Yinong, Cole, Wesley J, Maclaurin, Galen J, Mehos, Mark S, and Turchi, Craig S. Thu . 2019 "The Potential Role of Concentrating Solar Power within the Context of DOE's 2030 Solar Cost Targets". United States, pp. 1-137, doi:10.2172/1491726.

[37] S. Touili, A. A. Merrouni, A. Azouzoute, Y. El Hassouani, A. Amrani, A technical and economical assessment of hydrogen production potential from solar energy in Morocco, International Journal of Hydrogen Energy, Volume 43, Issue 51, 2018, Pages 22777-22796, ISSN 0360-3199, doi:10.1016/j.ijhydene.2018.10.136.

[38] P. Ineichen, 2008. Conversions function between the Linke turbidity and the atmospheric water vapor and aerosol content. Solar Energy, 82(11), pp.1095-1097.

[39] Beyoud, A., Hassanain, N. and Bouhaouss, A., 2018. Numerical Evaluation of Solar Irradiance Attenuation for Concentrating Solar Power Systems. International Journal of Renewable Energy Research (IJRER), 8(3), pp.1430-1441.

[40] Thomas, C., Wey, E., Blanc, P., Wald, L. and Lefèvre, M., 2016. Validation of HelioClim-3 version 4, HelioClim-3 version 5 and MACC-RAD using 14 BSRN stations. Energy Procedia, 91, pp.1059-1069.

[41] G. N. Reddy, S. Shrestha, B. Acharya, V. K. T. Bangi and R. Guduru, "Analysis of Hydrogen Dry Cell for Alkaline Water Electrolysis," 2018 7th International Conference on Renewable Energy Research and Applications (ICRERA), Paris, 2018, pp. 687-692. doi: 10.1109/ICRERA.2018.8566705.

[42] A. Bensenouci, & A. Medjelled, (2016). Thermodynamic and efficiency analysis of solar steam power plant cycle. International Journal of Renewable Energy Research, 6(4), 1556-1564.

[43] M.E. Hanyak, 2012. Chemical process simulation and the Aspen HYSYS software. Department of Chemical Engineering, Bucknell University.

[44] A. Moisseytsev, and J.J. Sienicki, 2008. Performance improvement options for the supercritical carbon dioxide Brayton cycle (No. ANL-GENIV-103). Argonne National Lab. (ANL), Argonne, IL (United States) pp. 1-52, doi: 10.2172/935094.

[45] V. Dostal, M.J. Driscoll, and P. Hejzlar, 2004. A supercritical carbon dioxide cycle for next generation nuclear reactors (Doctoral dissertation, Massachusetts Institute of Technology, Department of Nuclear Engineering), Vol.154, pp.1-326.

[46] M. Siddiqui, and K. Almitani, 2019. Energy Analysis of the S-CO_2 Brayton Cycle with Improved Heat Regeneration. Processes, 7(1), p.3.

[47] E.J. Sheu, and A. Mitsos, 2013. Optimization of a hybrid solar-fossil fuel plant: Solar steam reforming of methane in a combined cycle. Energy, 51, pp.193-202.

[48] A. Segal and M. Epstein, "Comparative performances of 'tower-top' and 'tower-reflector' central solar receivers," Sol. Energy, vol. 65, no. 4, pp. 207–226, 1999.

[49] System Advisor Model Version 2017.9.5 (SAM 2017.9.5) Website. Simple Efficiency Module. National Renewable Energy Laboratory. Golden, CO. Accessed September 23, 2017. https://sam.nrel.gov/content/simple-efficiency-module.

[50] A. Beyoud, A. Bouhaouss and N. Hassanain, "Impact of Anthropogenic Aerosols on Solar Beam Radiation Serving CSP Fields (Heliostat) in Morocco," 2018 6th International Renewable and Sustainable Energy Conference (IRSEC), Rabat, Morocco, 2018, pp. 1-4. doi: 10.1109/IRSEC.2018.8702982.